December 1, 2002

Cell Population Modelling of Yeast Glycolytic Oscillations

Michael A Henson, *University of Massachusetts - Amherst*
Dirk Muller
Matthias Reuss

Cell population modelling of yeast glycolytic oscillations

Michael A. HENSON*[1], Dirk MÜLLER† and Matthias REUSS†

*Department of Chemical Engineering, University of Massachusetts, Amherst, MA 01003, U.S.A., and †Institute of Biochemical Engineering, University of Stuttgart, 70569 Stuttgart, Germany

We investigated a cell-population modelling technique in which the population is constructed from an ensemble of individual cell models. The average value or the number distribution of any intracellular property captured by the individual cell model can be calculated by simulation of a sufficient number of individual cells. The proposed method is applied to a simple model of yeast glycolytic oscillations where synchronization of the cell population is mediated by the action of an excreted metabolite. We show that smooth one-dimensional distributions can be obtained with ensembles comprising 1000 individual cells. Random variations in the state and/or structure of individual cells are shown to produce complex dynamic behaviours which cannot be adequately captured by small ensembles.

Key words: cell-ensemble model, cell population dynamics, oscillatory dynamics, synchronization.

INTRODUCTION

The individual cell remains the major focus of biological and biochemical-engineering research. While single cells are of undeniable importance, cell cultures actually consist of millions of individual cells which are subject to random variations in their internal structure and state. Therefore a property such as the intracellular concentration of a particular metabolite is described by a distribution function rather than a scalar value. A typical biochemical measurement represents an average of the individual cell properties. In some applications, it is desirable to measure the distribution of a particular property across the cell population using a more sophisticated technique such as flow cytometry [1]. This motivates the development of models that capture the variations inherent in a large population of individual cells.

Single-cell models (SCMs) have been developed for several micro-organisms, plant cells and animal cells. For simple micro-organisms, such as *Escherichia coli*, where the genome has been completely sequenced, very detailed steady-state models consisting of hundreds of intracellular reactions and metabolites have been presented [2]. The development of dynamic SCMs is more challenging, owing to the difficulties associated with determining the intracellular reaction rates. Dynamic models of reasonable complexity have been presented for simple micro-organisms such as *Saccharomyces cerevisiae* [3,4]. Despite their sophistication, SCMs are not well suited for predicting average properties of random cell populations and are completely incapable of generating cell-distribution predictions.

A modelling framework that is well suited for capturing variations in a cell population is based on the population-balance equation (PBE). The basic theory of cell PBE modelling was developed over 30 years ago by Fredrickson and co-workers [5,6]. The dynamic PBE describes the number distribution of internal cell states as a function of time. Most models are based on a single internal state such as cell age [7] or cell mass [8]. Even for these relatively simple models, determination of the kernels which represent the rates of cell growth and division, substrate consumption and product formation is a formidable problem even if flow-cytometric data is available [1,9]. Cell PBE models characterized by a vector of internal states such as intracellular concentrations also can be constructed [10]. Nielsen and Villadsen [11] showed that the incorporation of intracellular reactions within the PBE framework is facilitated by utilizing a distribution function that represents the mass fraction of cells with a particular internal state. An inherent limitation of the PBE approach is that the incorporation of a detailed intracellular reaction network leads to a computationally intractable model because a high-dimensional distribution function must be computed.

Shuler and co-workers [12–15] have developed a computationally tractable alternative for modelling cell populations subject to random variations. Rather than formulate the governing PBE, the cell population is described by an ensemble of SCMs which differ according to key properties, such as the division size. A key advantage of the ensemble approach is that the number distribution function of any property captured by the SCM can be calculated by appropriate manipulation of the ensemble information. Ensembles with approx. 250 individual cells have been used to predict steady-state and transient size distributions for aerobic [14,15] and anaerobic [12] continuous cultures of *E. coli* as well as plasmid stability in a genetically modified *E. coli* strain [13]. Surprisingly, we have not found any recent developments or applications of this promising approach.

The cell-ensemble approach is based on the implicit assumption that the continuum limit represented by the PBE model can be approximated by a sufficiently large number of individual cells. This assumption is difficult to verify as the PBE model cannot be solved for most problems of practical interest. In this sense, the problem is similar to that commonly faced in the solution of partial differential equations by spatial discretization methods where a 'converged' solution is obtained by increasing the number of discretization points until the solution remains effectively unchanged [16]. In the present setting, the individual cells play the role of the discretization points.

In the present paper we continue the development of the ensemble approach for modelling cell behaviour at the population level. Unlike previous work by Shuler and co-workers [12–15], our focus is on the prediction of cell population synchronization for yeast glycolytic oscillations using a comparatively large

Abbreviations used: BPG, 1,3-bisphosphoglycerate; CPU, central processing unit; DHP, dihydroxyacetone phosphate; G3P, glyceraldehyde 3-phosphate; ODEs, ordinary differential equations; PBE, population-balance equation; PFK, phosphofructokinase; SCM, single-cell model.

[1] To whom correspondence should be addressed (e-mail henson@ecs.umass.edu).

number of individual cell models. We use the term 'single-cell model' to represent a metabolic model capable of predicting glycolytic oscillations at the single-cell level rather than a more complete model which accounts for cell-cycle events such as cell division [14,15].

The remainder of the present paper is organized as follows. First, previous experimental and modelling work on yeast glycolytic oscillations is reviewed. Next the cell-ensemble model for glycolytic oscillations based on previous work by Wolf and Heinrich [17] is presented and compared with a rigorous PBE model. Then the main results and discussion are presented. The paper concludes with a brief summary and a discussion of future research directions. Computational issues such as the numerical solution of large ensemble models and calculation of cell distribution properties are described in the Appendix.

YEAST GLYCOLYTIC OSCILLATIONS

Glycolysis is the cellular process by which glucose is metabolized to generate energy in the form of ATP. Because of its presence in a wide variety of organisms, this biochemical pathway has been the subject of numerous experimental and modelling studies. A striking feature of glycolytic-pathway behaviour is that, under certain conditions, oscillations have been observed in various glycolytic intermediates, coenzymes and extracellular species. Whereas the majority of studies have focused on yeast cells, oscillations also have been observed in algae [18], muscle [19], heart [20] and tumour [21] cells. The biological significance of this behaviour has long been debated. Rapp [22] argues that oscillatory dynamics have the potential to enhance the efficiency of energy storage as compared with stationarity. Even if they serve no direct biological function, glycolytic oscillations represent a well characterized behaviour that is well suited for the study of cell population dynamics.

Experimental studies

Glycolytic oscillations have been studied using cell-free extracts of yeasts such as *Saccharomyces cerevisiae* [23], *S. carlsbergensis* [24] and *S. uvarum* [25]. In some of the earliest studies by Chance and co-workers [24,26], intracellular oscillations were observed by continuous monitoring of the NADH concentration via fluorimetry and by conducting assays of various glycolytic intermediates. These results suggested that an autocatalytic reaction involving the enzyme phosphofructokinase (PFK) is the main cause of glycolytic oscillations. However, the simplistic view that a single reaction in the glycolytic chain is solely responsible for the oscillatory behaviour has been challenged by Metabolic Control Analysis [27]. Additional experimental work was focused on characterizing the cellular mechanism which causes synchronization of individual cells such that they oscillate in phase, thereby producing oscillations which are observable at the cell population level. Studies by Chance and co-workers [28] suggest that an extracellular metabolite excreted by the cells mediates the synchronization.

More recently, experiments involving intact cell populations of *S. cerevisiae* have been performed. Some of the most important studies have been conducted by Westerhoff and co-workers [29,30]. Their experimental procedure involves harvesting of batch-grown cells near the shift from glucose to ethanol as the growth substrate followed by immediate quenching with methanol at $-40\,^{\circ}C$. The suspended cells are introduced to an anaerobic stirred curvette, and oscillations are induced by adding glucose and KCN in succession. Sustained oscillations have been observed in the coenzyme NADH, glycolytic intermediates such as glucose 6-phosphate, fructose 6-phosphate and fructose 1,6-bisphosphate and extracellular species such as ethanol and acetaldehyde. The appearance of oscillations only after the addition of KCN is notable because cyanide is known to react with extracellular acetaldehyde. This observation, along with other experimental results, strongly suggests that acetaldehyde is the extracellular species responsible for synchronization of individual cells which leads to macroscopically observable oscillations [29,31].

Dynamic cell models

Many investigators have developed dynamic SCMs in an attempt to rationalize the glycolytic oscillations observed in yeast extracts and intact cells. Early models were based on different hypothesized mechanisms, including product activation of the enzyme PFK [32] and the autocatalytic stoichiometry of glycolysis [33]. Similar models have been proposed more recently [23,34,35]. The main advantage of these models is their simplicity, as only two or three non-linear ordinary differential equations (ODEs) are required to qualitatively describe the oscillatory dynamics. A shortcoming of such simple models is that they are based on *a priori* assignment of the oscillatory dynamics to a particular reaction in the glycolytic chain. Other researchers have argued that the idea of such an 'oscillaphore' is not internally consistent with the models themselves [27].

Recently, dynamic models based on more detailed descriptions of the glycolytic reaction chain have been proposed. Perhaps the most detailed model is that presented by Hynne et al. [3]. The model accounts for the transport of glucose, glycogen, ethanol, acetaldehyde and cyanide across the cell membrane, the degradation of acetaldehyde by cyanide, the storage of energy as ATP, basic cellular processes consuming ATP and eleven reactions between the glycolytic intermediates. For the computational studies pursued in the present paper, we have chosen to utilize the simpler cell model proposed by Wolf and Heinrich [17]. As discussed later, this model includes four glycolytic intermediates, three metabolites, the coenzyme pairs $NAD^+/NADH$ (more precisely $NAD^+/NADH + H^+$) and ATP/ADP, as well as transport of a combined pyruvate/acetaldehyde pool across the cell membrane. Although not investigated here, an extended version of this model with two additional glycolytic intermediates has been presented by Wolf et al. [36].

Regardless of their sophistication, individual cell models are not capable of explaining synchronization of the cell population that produces observable oscillations. Several investigators have developed cell-population models comprised of a small ensemble of individual cells in an attempt to describe the synchronization phenomenon. A common feature of most models is that the individual cells are coupled through the exchange of a metabolite (such as acetaldehyde) between the cells and the extracellular environment. Qualitative models can involve as few as two differential equations per cell [34,35]. More detailed mechanistic models based on the glycolytic reaction network also have been proposed [17,36]. The individual cell model and coupling mechanism proposed by Wolf and Heinrich [17] are used for the computational studies presented here. As described in more detail below, the coupling mechanism involves the transport of a combined acetaldehyde/pyruvate pool across the cell membranes and the degradation of extracellular acetaldehyde/pyruvate by reaction with cyanide. A model comprised of two interacting cells has been shown to produce complex dynamic behaviours including synchronous and asynchronous oscillations [17]. In the present study we utilize much larger cell ensembles to investigate the relationship between cell distribution properties and popu-

lation synchronization when individual cells are subject to random variations in their structure and/or state.

CELL-ENSEMBLE MODEL

We utilize the individual cell model for yeast glycolytic oscillations presented by Wolf and Heinrich [17] to illustrate the cell-ensemble-modelling approach. The cell model is derived from the simplified reaction pathway shown in Scheme 1. The anaerobic model accounts for glucose flux into the cell (J_0), consumption of glucose to produce intracellular glycerol, ethanol and a combined acetaldehyde/pyruvate pool, acetaldehyde/pyruvate flux out of the cell (J) and degradation of extracellular acetaldehyde/pyruvate by cyanide. Glycolytic intermediates are intracellular glucose (S_1), glyceraldehyde 3-phosphate/dihydroxyacetone phosphate (S_2), 1,3-bisphosphoglycerate (S_3) and intracellular acetaldehyde/pyruvate (S_4). Co-enzyme pairs involved in the pathway are NAD^+/NADH (N_1/N_2) and ADP/ATP (A_2/A_3). Because the pool of each co-enzyme pair is assumed to be conserved (AMP is neglected), only the NADH and ATP concentrations are treated as independent variables. The extracellular acetaldehyde/pyruvate pool concentration is denoted $S_{4,ex}$. Lumped intracellular reaction rates are denoted v_1–v_6, while the acetaldehyde/pyruvate degradation rate is denoted by v_7.

Model equations

The individual cell model derived from Scheme 1 and the extracellular coupling equation proposed by Wolf and Heinrich [17] are used in the subsequent computational studies. The differential equations describing the ith cell in the population is written as [17]:

$$\frac{dS_{1,i}}{dt} = J_0 - v_{1,i} = J_0 - k_1 S_{1,i} A_{3,i} \left[1 + \left(\frac{A_{3,i}}{K_I} \right)^q \right]^{-1} \quad (1)$$

$$\begin{aligned} \frac{dS_{2,i}}{dt} &= 2v_{1,i} - v_{2,i} - v_{6,i} \\ &= 2k_1 S_{1,i} A_{3,i} \left[1 + \left(\frac{A_{3,i}}{K_I} \right)^q \right]^{-1} \\ &\quad - k_2 S_{2,i}(N - N_{2,i}) - k_6 S_{2,i} N_{2,i} \end{aligned} \quad (2)$$

$$\frac{dS_{3,i}}{dt} = v_{2,i} - v_{3,i} = k_2 S_{2,i}(N - N_{2,i}) - k_3 S_{3,i}(A - A_{3,i}) \quad (3)$$

$$\frac{dS_{4,i}}{dt} = v_{3,i} - v_{4,i} - J_i = k_3 S_{3,i}(A - A_{3,i}) - k_4 S_{4,i} N_{2,i} - J_i \quad (4)$$

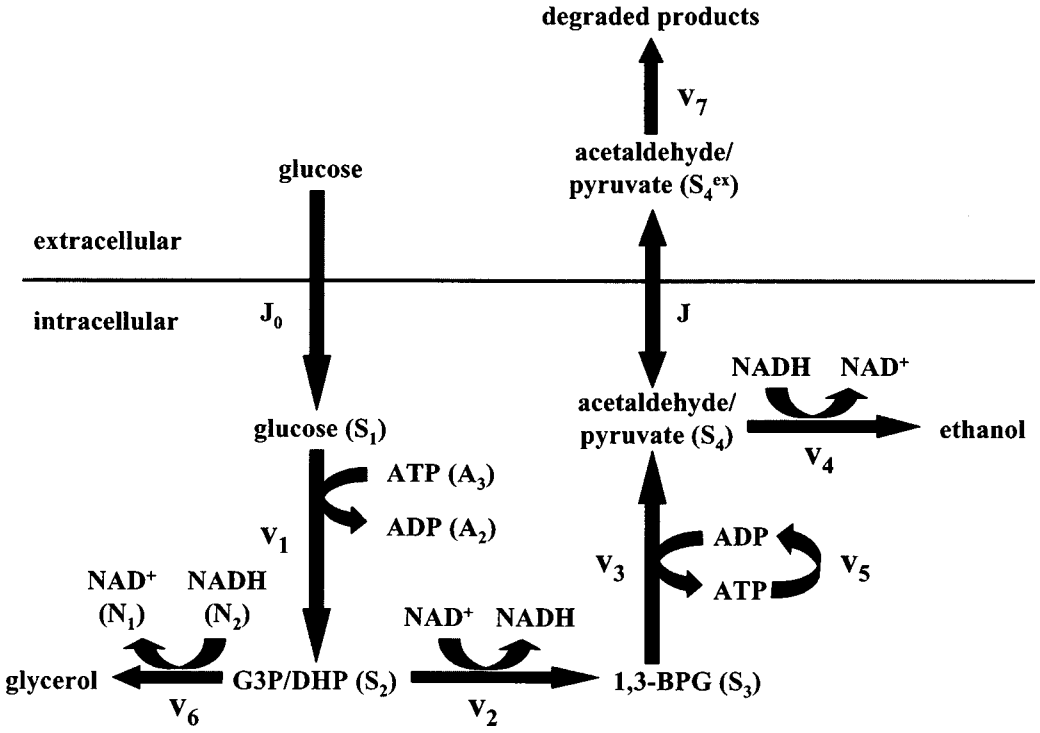

Scheme 1 Yeast glycolytic reaction pathway for anaerobic growth proposed by Wolf and Heinrich [17]

Extracellular glucose is assumed to be transported across the cellular membrane at a constant flux to produce intracellular glucose. Intracellular glucose is converted into two molecules of glyceraldehyde 3-phosphate (G3P)/dihydroxyacetone phosphate (DHP), and two molecules of ATP are consumed via a lumped reaction involving the enzymes hexokinase, phosphoglucoisomerase and phosphofructokinase. Glycerol is formed from the triose phosphates via a reaction that consumes one molecule of NADH. The enzyme glyceraldehyde-3-phosphate dehydrogenase catalyses a reaction which converts G3P/DHP into 1,3-bisphosphoglycerate (1,3-BPG) and produces one molecule of NADH. 1,3-BPG is converted into intracellular acetaldehyde/pyruvate, and two molecules of ATP are produced via a lumped reaction involving the enzymes phosphoglycerate kinase, phosphoglycerate mutase, enolase and pyruvate kinase. The ATP generated by this reaction is assumed to be consumed by non-glycolytic reactions. Ethanol is produced from the intracellular acetaldehyde/pyruvate by a reaction that consumes one molecule of NADH. Intracellular acetaldehyde/pyruvate is transported across the cellular membrane to produce extracellular acetaldehyde/pyruvate. Extracellular acetaldehyde/pyruvate is degraded by reaction with cyanide. The following nomenclature is used: J_0, glucose flux into the cell; J, acetaldehyde/pyruvate flux out of the cell; S_i, concentration of the ith intracellular species; A_2, concentration of ADP; A_3, concentration of ATP; N_1, concentration of NAD^+; N_2, concentration of NADH; v_j, rate of the jth intracellular reaction; $S_{4,ex}$, concentration of extracellular acetaldehyde/pyruvate; and v_7, rate of the acetaldehyde/pyruvate degradation reaction.

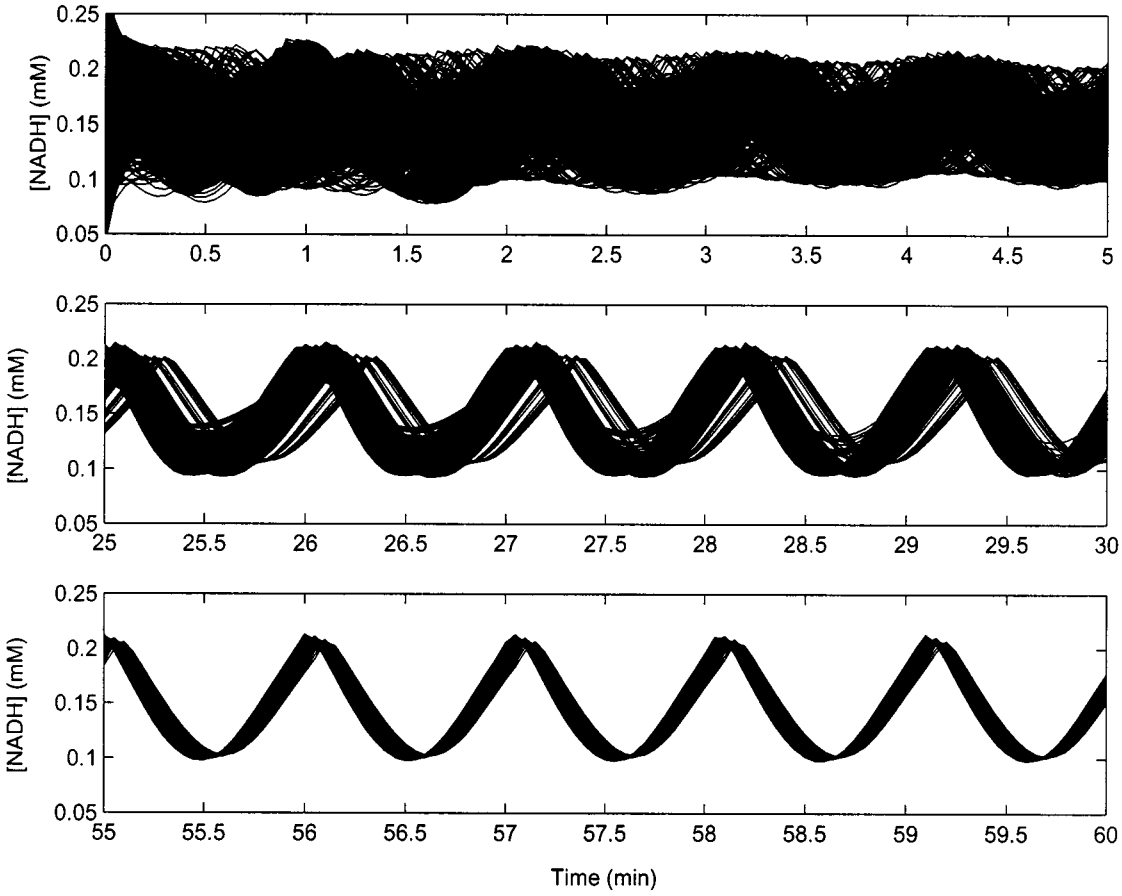

Figure 1 Cell-population synchronization for a 1000-cell ensemble in which the initial conditions of each cell are perturbed according to a Gaussian distribution with zero mean and a variance of 2.25

The plot shows the evolution of NADH concentration of each cell. The cell population becomes increasingly synchronized due to the coupling action of the excreted acetaldehyde/pyruvate pool.

$$\frac{dN_{2,i}}{dt} = v_{2,i} - v_{4,i} - v_{6,i}$$

$$= k_2 S_{2,i}(N - N_{2,i}) - k_4 S_{4,i} N_{2,i} - k_6 S_{2,i} N_{2,i} \quad (5)$$

$$\frac{dA_{3,i}}{dt} = -2v_{1,i} + 2v_{3,i} - v_{5,i} = -2k_1 S_{1,i} A_{3,i} \left[1 + \left(\frac{A_{3,i}}{K_I} \right)^q \right]^{-1}$$

$$+ 2k_3 S_{3,i}(A - A_{3,i}) - k_5 A_{3,i} \quad (6)$$

where S_1, S_2, S_3, S_4, N_2 and A_3 denote the intracellular concentrations of the intracellular species shown in Scheme 1; A and N denote the total concentration of the ADP/ATP and NAD^+/NADH pools respectively; J_0 is the flux of glucose into the cell; and J_i is the net flux of the acetaldehyde/pyruvate pool out of the cell. The intracellular reaction rates v_2–v_6 are assumed to depend linearly on the metabolite and coenzyme involved in each reaction. The expression for the intracellular reaction rate, v_1, includes an additional non-linear factor that accounts for inhibition by ATP.

The net flux of acetaldehyde/pyruvate from the ith cell into the extracellular environment is modelled as [17]:

$$J_i = \kappa(S_{4,i} - S_{4,ex}) \quad (7)$$

where $S_{4,ex}$ is the extracellular acetaldehyde/pyruvate concentration and κ is a coupling parameter related to the cell permeability. A mass balance on extracellular acetaldehyde/pyruvate is derived under the assumption that the volume fraction of cells relative to the total medium volume (φ) remains constant as the total number of cells, M, is varied [35]:

$$\frac{dS_{4,ex}}{dt} = \frac{\varphi}{M}\sum_1^M J_i - v_7 = \frac{\varphi}{M}\sum_1^M J_i - kS_{4,ex} \quad (8)$$

where k is the kinetic constant of the acetaldehyde/pyruvate degradation reaction. The total number of differential equations (n) in the cell-ensemble model increases linearly with the number of intracellular species (6) and the number of individual cells (M):

$$n = 6M + 1$$

Therefore a cell ensemble model has the potential to remain computationally tractable even when a large number of intracellular reactions are involved.

Model parameters

Unless stated otherwise, the model parameters used in the subsequent simulations have the values shown in Table 1. The parameter values are identical with those used by Wolf and

Table 1 Nominal values of the yeast-cell-ensemble-model parameters

Parameter	Value	Parameter	Value
J_0	2.30 mM · min^{-1}	κ	50.0 min^{-1}
k_1	100 mM^{-1} · min^{-1}	q	4.00
k_2	6.00 mM^{-1} · min^{-1}	K_I	0.520 mM
k_3	16.0 mM^{-1} · min^{-1}	N	1.00 mM
k_4	100 min^{-1}	A	4.00 mM
k_5	1.28 min^{-1}	φ	0.1
k_6	12.0 mM^{-1} · min^{-1}	M	1000
k	1.30 min^{-1}		

Heinrich [17], with the exception of the glucose flux, J_0, and the coupling parameter, κ. Wolf and Heinrich [17] note that their parameter values were chosen such that the metabolite concentrations remain in a reasonable range rather than being derived directly from data. The values for the parameters J_0 and κ were modified owing to the very slow synchronization that results with the original values [17]. We have achieved considerably more rapid synchronization consistent with that observed experimentally [28,31] by decreasing the glucose flux into each cell (J_0: $3.0 \rightarrow 2.3$ mM · min^{-1}) and by increasing the coupling between cells (κ: $13 \rightarrow 50$ min^{-1}).

Wolf and Heinrich [17] provide a very detailed investigation of two oscillating cells ($M = 2$) which have identical kinetic parameters. While such analysis has theoretical value, the implications for real cultures are debatable. In the present paper we utilize much larger cell ensembles ($M \approx 1000$) to study the relationship between cell distribution properties and population synchronization when individual cells are subject to random variations in their structure and/or state. For the nominal parameter values listed in Table 1, the cell-ensemble model possesses a single stable periodic solution in which all the cells oscillate in phase and with the same amplitude regardless of the cell number. Wolf and Heinrich [17] provide a detailed bifurcation analysis of such synchronous oscillations when $M = 2$. Substantially more complex asymptotic solutions are obtained when the cell ensemble model is comprised of many cells, each of which is subject to random perturbations. For this more realistic case, dynamic simulation is the most useful tool for characterizing model behaviour.

RESULTS AND DISCUSSION

The cell-ensemble-modelling approach is applied to the problem of yeast glycolytic oscillations to predict transient distribution properties of a partially synchronized cell population. The dynamic simulations utilize the nominal parameter values listed in Table 1. As mentioned above, for these parameters all cells oscillate in phase and with the same amplitude regardless of the cell number. Because all cells behave identically, the state of the cell ensemble at a particular instant of time is completely characterized by the six glycolytic intermediate concentrations of an individual cell and the extracellular concentration of the acetaldehyde/pyruvate pool. Table 2 shows a point from the periodic solution obtained with the parameter values in Table 1. The complete periodic solution can be reconstructed by integration of the cell ensemble model with this point as the initial condition.

Table 2 A point on the oscillatory solution corresponding to the model parameters in Table 1

Variable	Value	Variable	Value
S_1	1.023 mM	N_2	1.624×10^{-1} mM
S_2	6.696×10^{-1} mM	A_3	1.250 mM
S_3	7.194×10^{-2} mM	$S_{4,ex}$	8.419×10^{-2} mM
S_4	1.094×10^{-1} mM		

We focus on NADH concentration dynamics under conditions that result in partial synchronization or desynchronization of the cell population. The choice is motivated by a number of experimental studies where the average NADH concentration was continuously measured by fluorimetry to identify sustained oscillations consistent with a synchronized cell population [28,31,37]. The ensemble model produces non-trivial number distributions (i.e. cells with different NADH concentrations) only if there is some source of randomness in the individual cells. Two sources of randomness are considered in the following simulations. An initially unsynchronized population of cells is simulated by randomly perturbing the initial conditions. Random perturbation of the intracellular kinetic parameters is used to simulate a population of non-identical cells which is initially synchronized. We study the effects of randomness on the NADH ensemble average and number distribution. For simplicity, only univariate NADH number distributions are computed. The generalization to multidimensional distributions is more involved, but conceptually straightforward.

Comparison with a PBE model

The cell ensemble model is constructed under the implicit assumption that the continuum limit represented by a PBE model can be approximated by a sufficiently large number of individual cells. For the sake of illustration, a PBE model based on the glycolytic reaction network in Scheme 1 is formulated to evaluate the relative computational demands of cell ensemble and PBE modelling schemes. We utilize the PBE modelling formalism presented by Nielsen and Villadsen [11] because it allows intracellular reactions to be incorporated in a straightforward manner. The key distinction between this method and the more traditional approach developed by Fredrickson and coworkers [6] is that the transient distribution function represents the mass fraction rather than the number fraction of cells with a particular internal state.

The PBE is written as [11]:

$$\frac{\partial \Psi(x,t)}{\partial t} + \sum_{i=1}^{L} \frac{\partial}{\partial x_i}[R_i(x,t)\Psi(x,t)] = [\mu(x,t) - \mu(t)]\Psi(x,t) \tag{9}$$

where x is the internal state vector, t is time, $\Psi(x,t)\,dx$ represents the mass fraction of cells with internal state in the range $[x, x+dx]$ at time t, L is the number of intracellular species, x_i is the intracellular concentration of species i and $R_i(x,t)$ is the net rate of formation of species i. The function $\mu(x,t)$, which represents the specific growth rate of cells with internal state x, is calculated as:

$$\mu(x,t) = \sum_{i=1}^{L} \sum_{j=1}^{J} \gamma_{ij} r_j(x,t) \tag{10}$$

where J is the number of intracellular reactions, γ_{ij} is the stoichiometric coefficient for the ith species in the jth intracellular reaction; and $r_j(x,t)$ is the rate of the jth reaction. The average specific growth rate, $\mu(t)$, is computed by integrating $\mu(x,t)$ over the distribution:

$$\mu(t) = \int_0^{\infty} \mu(x,t)\Psi(x,t)\,dx \tag{11}$$

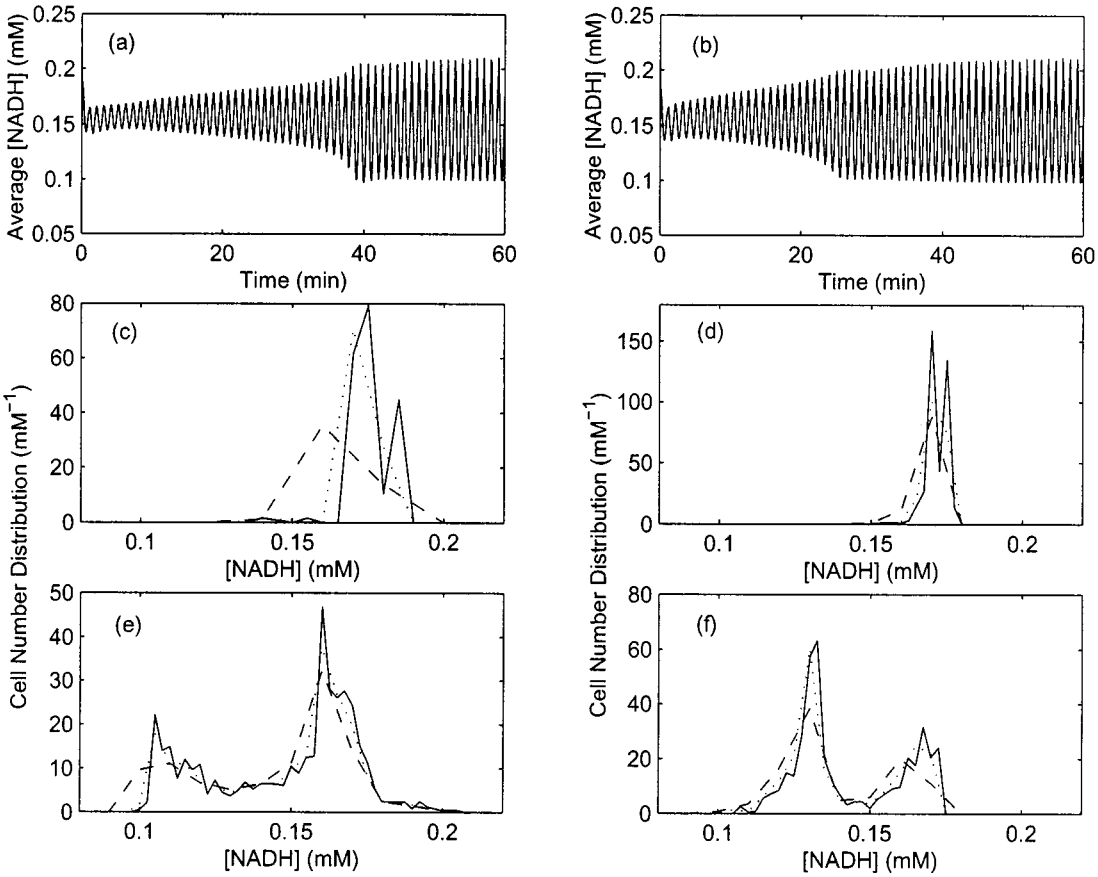

Figure 2 Cell-population synchronization for 250- and 1000-cell ensembles in which the initial conditions are perturbed according to a Gaussian distribution with zero mean and a variance of 2.25

Plots (**a**) and (**b**) show the evolution of the average NADH concentration for the 250- and 1000-cell ensembles respectively. The 250-cell ensemble shows slower convergence to fully developed oscillations. Plots (**c**) and (**d**) show NADH number distributions computed from the 250- and 1000-cell ensembles respectively at 60 min with $z_0 = 0$ mM and $z_L = 0.3$ mM. Three interval widths [$\Delta z = 0.02$ mM (——), 0.01 mM (· · · ·) and 0.005 mM (-- -- -- --)] are shown for each ensemble. The 250-cell ensemble does not provide satisfactory resolution of the NADH variations in the cell population. Plots (**e**) and (**f**) show NADH number distributions computed from the 1000-cell ensemble at times $t = 5$ and 30 min respectively with $z_0 = 0$ mM and $z_L = 0.3$ mM. Three interval widths $\Delta z = 0.02$ mM (——), 0.01 mM (· · · ·) and 0.005 mM (-- -- -- --) are shown for each time. The number distributions show the presence of two cell subpopulations which eventually become synchronized and converge into a single population that produces fully developed oscillations.

For the yeast glycolytic pathway depicted in Scheme 1, the number of intracellular species $L = 6$, where $x^T = [S_1 S_2 S_3 S_4 N_2 A_3]$, and the number of intracellular reactions $J = 6$ where $r^T = [v_1 v_2 v_3 v_4 v_5 v_6]$. Note that only the stoichiometry and the rates of the intracellular reactions are needed to completely specify the functions in the PBE. The model also will require a mass balance on the extracellular acetaldehyde/pyruvate pool.

Rather than pursue a complete formulation of the PBE model, we show that the resulting model is computationally intractable if the internal cell state is discretized using standard procedures such as finite differences [38], finite elements [39] or orthogonal collocation [40]. The key point is that the internal state, x, which characterizes the intracellular concentrations of each cell, is of dimension six. Assume the model is to be solved numerically by discretization in each of the six internal co-ordinates. This procedure will yield a set of coupled non-linear ODEs with time as the only independent variable. If the same number of discretization points, m, is used for each co-ordinate, the total number of ODEs derived from the PBE will be $n = m^6$. Even with a very coarse discretization where $m = 10$, this procedure results in one million ODEs. While it can be argued that more sophisticated solution techniques are available [9,41], the dimension of the internal state vector clearly places severe limitations on the complexity of the intracellular reaction network that can be utilized. For example, the yeast glycolysis model described by Hynne et al. [3] has an internal state vector of dimension 15. The development of improved numerical solution techniques for such high-dimensional PBE models is unlikely to be successful with current computing technology. By contrast, the number of ODEs in the cell-ensemble model increases linearly with the dimension of the internal cell state.

Cells with randomized initial conditions

The first set of dynamic simulation tests involves cell ensembles of different sizes in which the initial condition of each cell is randomly perturbed from the nominal values in Table 2. The initial conditions are perturbed according to a Gaussian distribution with zero mean and a variance of 2.25. Figure 1 shows the evolution of the NADH concentration of each individual cell in an ensemble of 1000 identical cells. While the behaviour of any particular cell cannot be easily distinguished, the degree of synchronization is clearly evident. Owing to the large variance used, initially the cell population is highly disorganized and

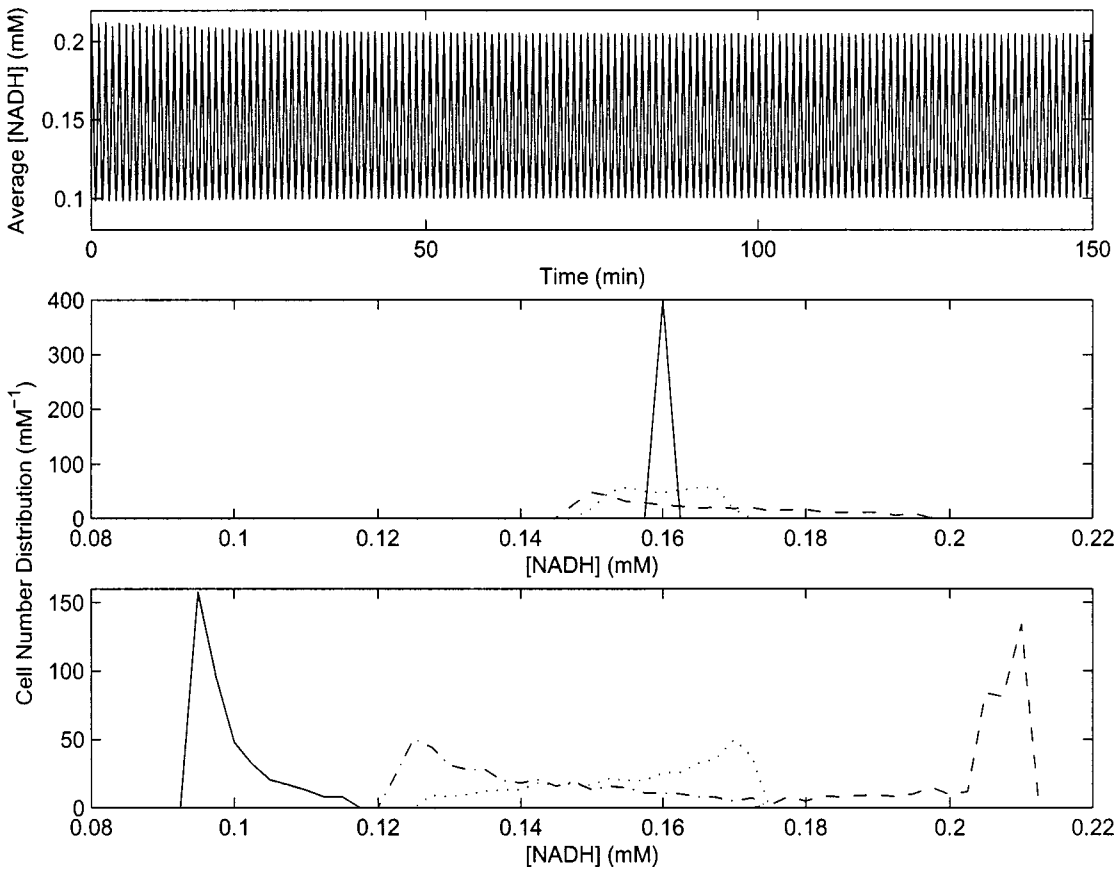

Figure 3 Partial cell-population desynchronization for 1000-cell ensemble with random perturbations of variance 1×10^{-4} in the intracellular reaction rate constants k_1–k_6

The top plot shows that these small intracellular variations have very little effect on the dynamics of the average NADH concentration. The middle plot shows the computed NADH number distributions at 0 (——), 10 (· · · ·) and 150 (– – – –) min. The discretization interval is 0.0025 mM with low and high values of 0.08 mM and 0.22 mM respectively. The random variations cause a very substantial dispersion of the cell population. The bottom plot shows the computed NADH number distributions over a single oscillation period corresponding to the last complete cycle shown in the top plot. The four lines represent the distributions at the bottom of the oscillation (——), in the middle of the oscillation going upward (· · · ·), at the top of the oscillation (– – – –) and in the middle of the oscillation going downward (–·–·). The distribution pairs corresponding to the two extremes and the two midpoints are symmetric.

exhibits no temporal structure indicative of a synchronized culture. After 25 min the population becomes quite synchronized through the coupling effect of the extracellular acetaldehyde/pyruvate. A highly synchronized population in which the cells oscillate in phase and with a period of approx. 1 min is observed after 60 min.

Figure 2 depicts the dynamic behaviour of the NADH concentration for two different ensembles consisting 250 and 1000 individual cells. For each ensemble, the initial conditions are perturbed according to a Gaussian distribution with zero mean and a variance of 2.25. Figures 2(a) and 2(b) show the evolution of the average NADH concentration computed from the 250 and 1000 cell ensembles respectively. The average behaviour obtained with 1000 cells is consistent with the full ensemble behaviour shown in Figure 1 in that partial synchronization (as indicated by large amplitude oscillations) is evident after 25 min and nearly complete synchronization (as indicated by almost completely developed oscillations) is achieved after 55 min. The relatively slow convergence to fully develop oscillations obtained with 250 cells indicates that the synchronization effect is less pronounced than that observed with the 1000-cell ensemble. When drawing such conclusions it is important to recognize that different dynamic responses are expected, both due to the difference in cell number and the random nature of the initial conditions. Because the same trend has been observed for a number of random initial conditions, this result shows that the cell number can have a strong effect on the average population dynamics, even for this simple glycolysis model.

Figures 2(c) and 2(d) show NADH number distributions computed from the 250 and 1000 cell ensembles respectively at 60 min. The NADH concentration is discretized into intervals of width Δz with minimum value $z_0 = 0$ mM and maximum value $z_L = 0.3$ mM. Three interval widths $\Delta z = 0.02$, 0.01 and 0.005 mM are shown for each ensemble. As compared with the 1000-cell-ensemble results, the computed number distributions for 250 cells do not provide adequate resolution of the NADH variations in the cell population. These comparisons demonstrate key shortcomings of using small cell ensembles such as those studied by Wolf and Heinrich [17] to simulate the dynamics of real cultures.

Figures 2(e) and 2(f) show NADH number distributions computed from the 1000-cell ensemble at times $t = 5$ and 30 min respectively. Three interval widths $\Delta z = 0.01$, 0.005 and 0.0025 mM are shown for each time. When viewed with Figure 2(d), these two Figures show the presence of two cell subpopulations which eventually become synchronized and converge into

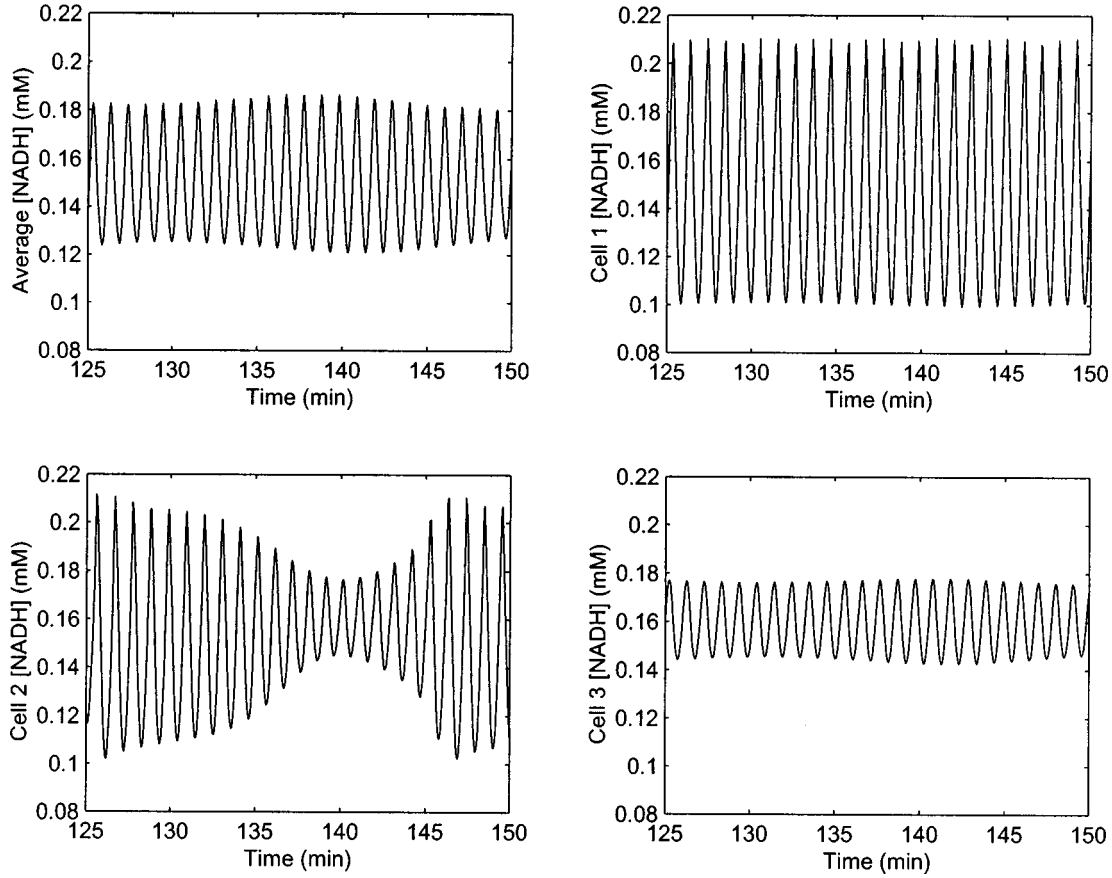

Figure 4 Partial cell-population desynchronization for 1000 cells with random perturbations of variance 6.25×10^{-4} in the intracellular reaction rate constants k_1–k_6

The plot shows the evolution of the average NADH concentration and the NADH concentration of three individual cells at the end of the 150 min simulation. The average NADH value shows that this extent of intracellular variation leads to significant desynchronization of the cell population. The three individual cells are chosen to show the oscillatory dynamics of representative cells from three distinct subpopulations. A sufficiently large ensemble is required to populate the three subpopulations such that satisfactory predictions of average and distribution properties are obtained.

a single population that produces fully developed oscillations. One subpopulation corresponds to a large group of cells that quickly converges to the final periodic solution. The second population corresponds to a smaller group of cells that initially exhibits small amplitude oscillations before eventually converging to the larger amplitude oscillations. Note that significant information is lost when the interval width $\Delta z = 0.01$ mM (30 intervals for this case) is used. By contrast, good results are obtained for $\Delta z = 0.005$ and 0.0025 mM. Although some noise is evident in Figure 2(e), we utilize $\Delta z = 0.0025$ mM (120 intervals for this case) for subsequent analysis because this value provides the best resolution of the two cell subpopulations.

Although not shown here, we also have simulated the population dynamics of a 5000-cell ensemble with randomly perturbed initial conditions. The dynamic response of the average NADH concentration is virtually indistinguishable from that obtained for the 1000-cell ensemble. Distributions generated from the 5000-cell ensemble data provide slightly better resolution than those obtained for the 1000-cell ensemble. With the exception of some noise in the distributions for the 1000-cell ensemble, both sets of results are equally satisfactory when $\Delta z = 0.0025$ mM. On the other hand, the dynamic simulation for the 5000-cell ensemble requires well over 1 h of central-processing-unit (CPU) time, while less than 10 min are necessary for the 1000-cell ensemble. Consequently we utilized a 1000-cell ensemble and $\Delta z = 0.0025$ in the subsequent simulation studies.

Cells with randomized kinetic parameters

The second set of simulation tests involves ensembles of 1000 cells in which the intracellular reaction rate constants k_1–k_6 are randomly perturbed from their nominal values in Table 1. The other intracellular model parameters (K_I, q, N and A) are held fixed at their nominal values. These simulations are designed to test the robustness of the synchronization mechanism to variations in individual cells which invariably exist in a real population. Due to lack of experimental data concerning the expected amount of variation, the intracellular kinetic parameters are randomly perturbed to produce varying extents of desynchronization. Actual cell populations may produce synchronization despite significantly greater variations due to the presence of other stabilizing effects not included in the simple glycolysis model studied here. The dependent variable values listed in Table 2 corresponding to a point on the periodic solution for 1000 identical cells are used as the initial conditions. NADH number distributions are computed with $z_0 = 0.08$ mM, $z_L = 0.22$ mM and $\Delta z = 0.0025$ mM.

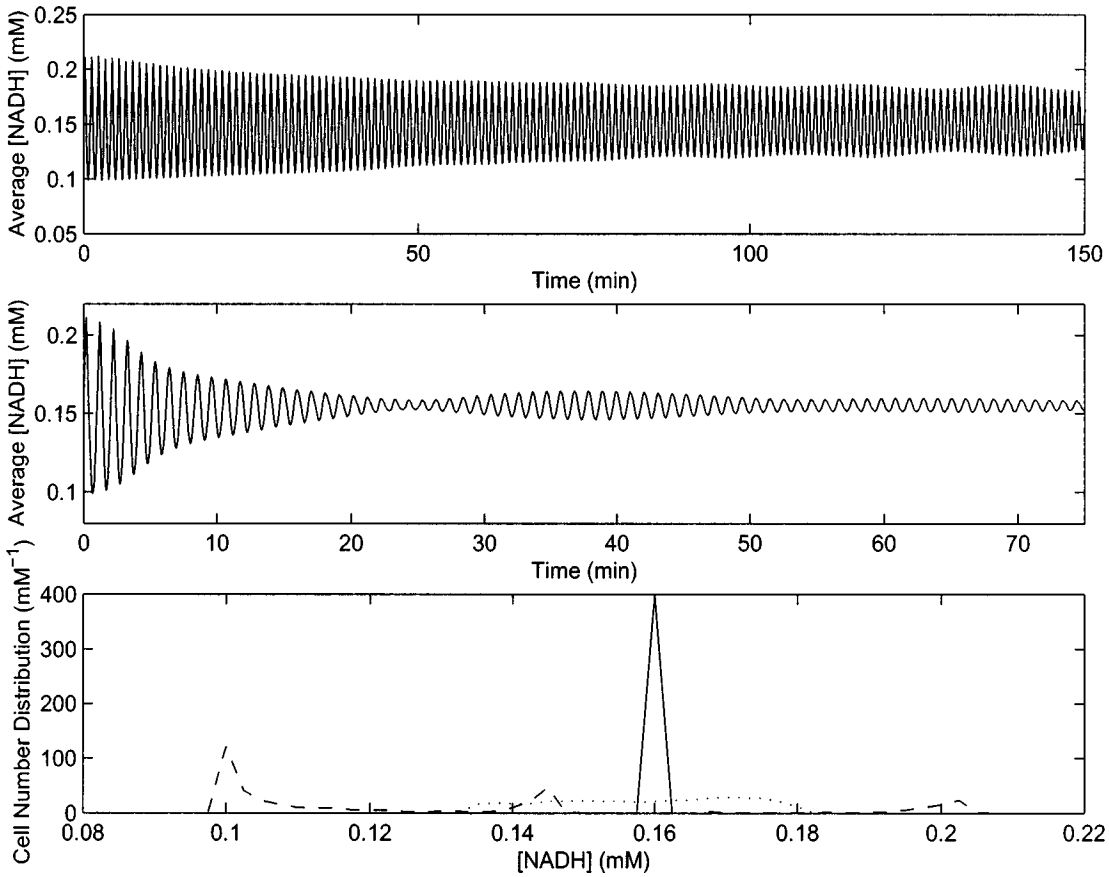

Figure 5 Partial cell-population desynchronization for 1000 cells with larger random perturbations in the intracellular reaction rate constants k_1–k_6

The top and middle plots show the evolution of the average NADH concentration for a variance of 6.25×10^{-4} and 1×10^{-2} respectively. The larger perturbation overwhelms the extracellular coupling mechanism and leads to almost complete desynchronization. The bottom plot shows computed NADH number distributions at 0 (——), 10 (· · · ·) and 150 (– – – –) min when the variance is 6.25×10^{-4}. The discretization interval is 0.0025 mM with low and high values of 0.08 mM and 0.22 mM respectively. The final distribution shows the existence of the three distinct cell subpopulations.

The cell-ensemble model exhibits very little robustness to intracellular variations when the parameter values proposed by Wolf and Heinrich [17] are utilized. Perturbations significantly smaller than those considered below lead to almost complete desynchronization of the cell population. As discussed previously, we constructed an improved model by increasing the coupling between cells (κ: $13 \rightarrow 50$ min^{-1}) and by decreasing the glucose flux into each cell (J_0: $3.0 \rightarrow 2.3$ mM · min^{-1}). Extensive simulation results not shown here demonstrate that κ is the key parameter that determines the degree of synchronization which results from randomization of the intracellular kinetics. Because increasing κ also has undesirable effects such as reducing the amplitude of the glycolytic oscillations, the parameter value chosen represents an acceptable balance between multiple effects.

The top plot in Figure 3 shows the evolution of the average NADH concentration computed from a 1000-cell ensemble in which the kinetic parameters are randomly perturbed with zero mean and variance of 1×10^{-4}. From the perspective of the average ensemble behaviour, these small intracellular variations have very little effect. The middle plot shows the NADH number distributions computed at $t = 0$, 10 and 150 min. Surprisingly, the small decrease in the oscillation amplitude of the average NADH concentration is accompanied by a very substantial dispersion of the cell population. This result suggests that average population measurements can provide misleading information about the underlying population behaviour. More informative data can be obtained via a measurement technique such as flow cytometry [1], which provides the distribution of intracellular properties across the population. The bottom plot shows NADH number distributions computed over a single oscillation period corresponding to the last complete cycle in the top plot. All four distributions are resolved satisfactorily and the amount of noise is very low. Relatively sharp distributions are obtained at the two extremes of the oscillation, while more dispersed distributions are produced at the midpoints. Symmetry of the distribution pairs corresponding to the two extremes and the two midpoints is clearly evident. This provides further evidence that the chosen discretization parameters are adequate.

The next simulation test involves a 1000-cell ensemble in which the kinetic parameters are randomly perturbed with zero mean and variance of 6.25×10^{-4}. This amount of variation leads to significant desynchronization of the cell population. While the resulting dynamic behaviour is not easily characterized, the random variations produce three distinct cell subpopulations. This behaviour is depicted in Figure 4, where the dynamics of the average NADH concentration and the NADH concentration of three individual cells near the end of the 150 min simulation are shown. In addition to being slightly irregular, the amplitude of the average NADH concentration oscillations is significantly reduced as compared with that observed for a population of

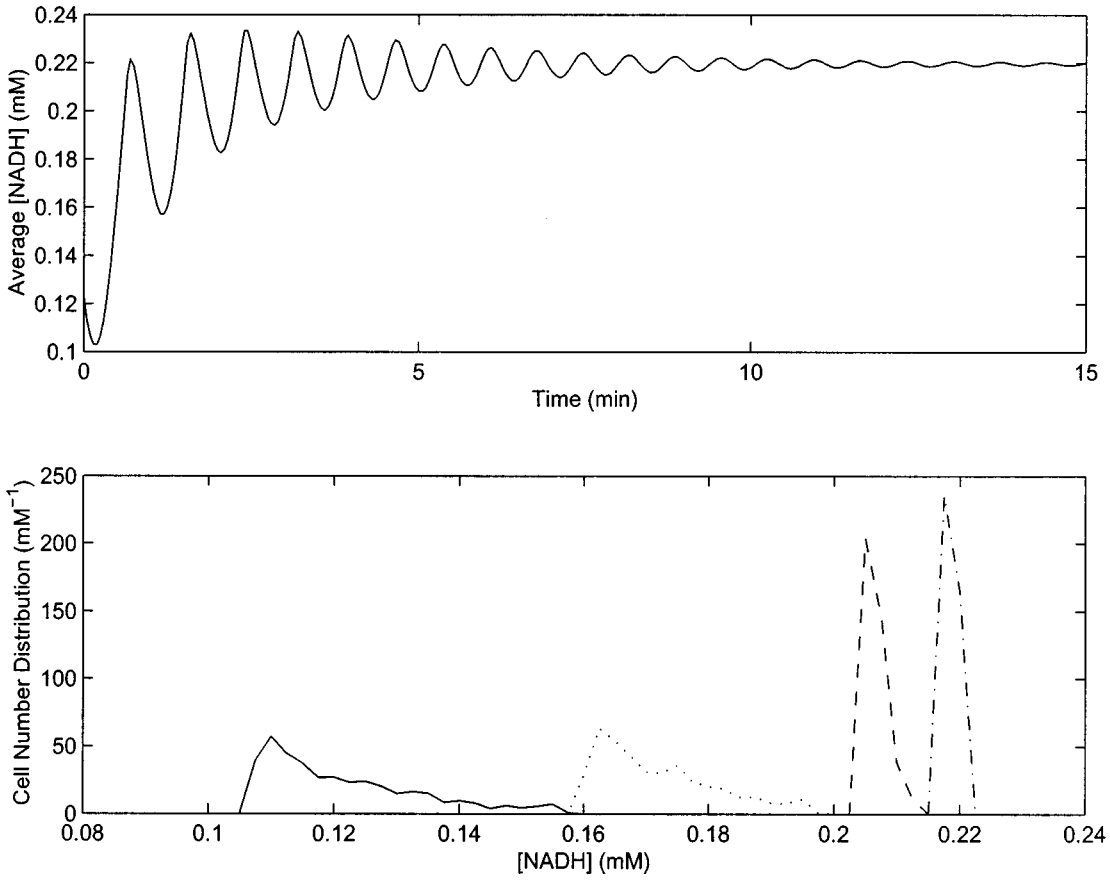

Figure 6 Damped oscillations that occur due to a decrease in cell concentration from 0.1 to 0.02 at $t = 0$ min for 1000 cells with random perturbations of variance 1×10^{-4} in the intracellular reaction rate constants k_1–k_6

The top plot showing the evolution of the average intracellular NADH concentration demonstrates that the lower cell concentration does not support sustained oscillations. The bottom plot shows computed NADH number distributions at 0 (——), 1 (· · · ·) and 5 (– – – –) and 15 (–·–·) min for a discretization interval of 0.0025 mM and low and high values of 0.08 mM and 0.25 mM respectively. The sharpening of the number distribution with time is attributable to the NADH concentration of each cell converging to a constant value.

identical cells. The three individual cells are chosen to more explicitly show the oscillatory dynamics of representative cells from the three subpopulations. The first cell produces sustained oscillations of constant and relatively large amplitude. The second cell exhibits more complex behaviour where the oscillation amplitude periodically varies between relatively small values and larger values similar to that of the first cell. The third cell produces sustained oscillations of constant, but relatively small, amplitude. Each of the three subpopulations must contain a sufficient number of cells to yield accurate predictions of average and distribution properties. This is possible only if the cell ensemble is relatively large.

The top and middle plots in Figure 5 show the evolution of the average NADH concentration for a 1000-cell ensemble in which the intracellular kinetic parameters have a variance of 6.25×10^{-4} and 1×10^{-2} respectively. The smaller perturbation results in only partial desynchronization of cell population, while the larger perturbation leads to almost complete desynchronization. This result demonstrates that the extracellular coupling mechanism offers limited robustness to intracellular variations. The bottom plot shows NADH number distributions computed at $t = 0$, 10 and 150 min for the 1000-cell ensemble in which the intracellular kinetic parameters have a variance of 6.25×10^{-4}. The sharp initial distribution is indicative of a highly synchronized cell population. As random cell variations lead to partial desynchronization, the NADH distribution becomes increasingly dispersed. The final distribution clearly shows the existence of the three distinct cell subpopulations depicted in Figure 4. Although not shown here, NADH number distributions computed when the intracellular kinetic parameters have a variance of 1×10^{-2} show increasing dispersion that reflects the lack of any further temporal organization at the cell population level.

Further tests with randomized cells

The final simulation tests are designed to examine cell population behaviour under environmental conditions investigated in previous experimental studies [28,31,37]. We consider ensembles of 1000 cells in which the reaction rate constants k_1–k_6 are randomly perturbed with zero mean and variance of 1×10^{-4} from their nominal values in Table 1. For each test, the initial condition represents a point on the oscillatory solution that results when the cell-ensemble model with randomized parameters is integrated until the asymptotic solution is achieved. Unless explicitly stated otherwise, the same set of initial conditions and randomized model parameters are used for each test. As before, NADH number distributions are computed with $z_0 = 0.08$ mM, $z_L = 0.22$ mM and $\Delta z = 0.0025$ mM.

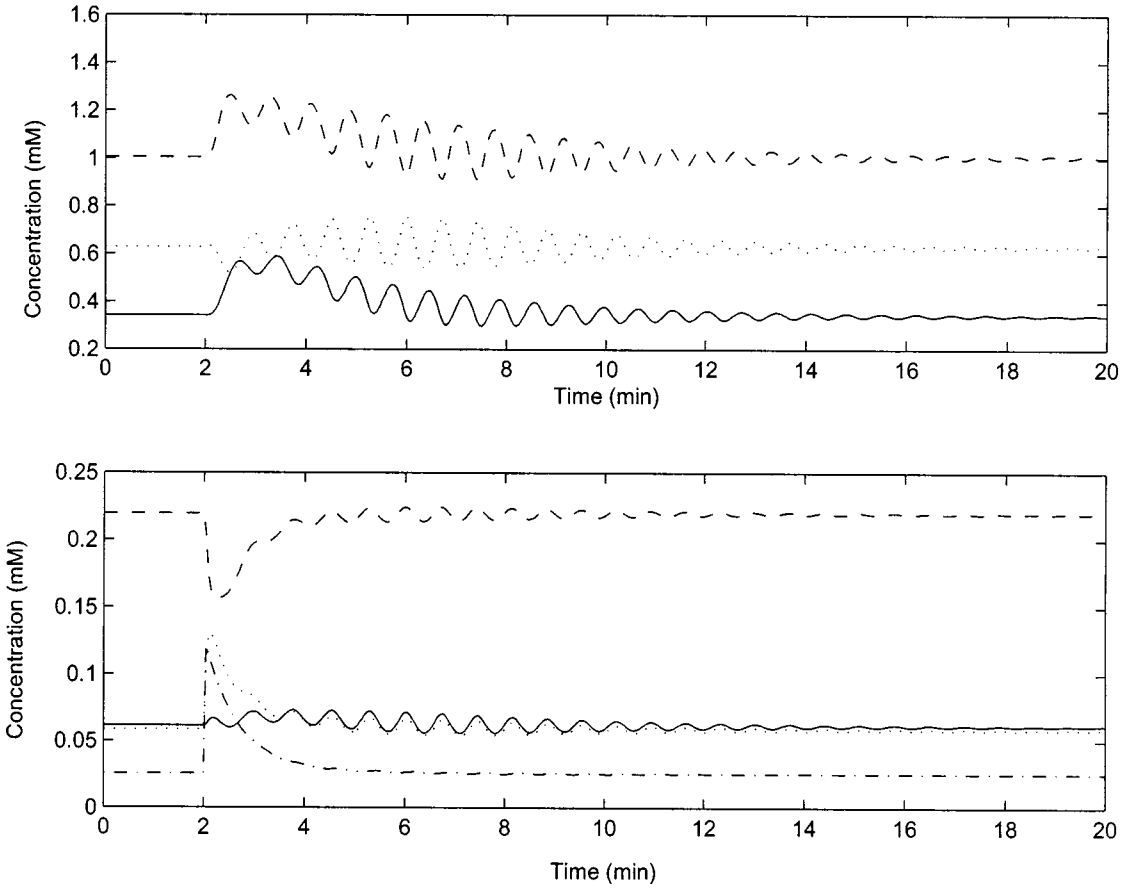

Figure 7 Damped oscillations that occur due to a 0.1 mM acetaldehyde/pyruvate pulse at $t = 2$ min for 1000 cells with random perturbations of variance 1×10^{-4} in the intracellular reaction rate constants k_1–k_6 and a cell concentration of 0.02

The top plot shows the evolution of the average S_1 (——), S_2 (· · · ·) and A_3 (– – – –) concentrations. The bottom plot shows the evolution of the average S_3 (——), S_4 (· · · ·) and N_2 (– –) concentrations and the $S_{4,ex}$ (– · – ·) concentration. The oscillations are not sustained because the extracellular acetaldehyde/pyruvate concentration converges to a constant value.

Figure 6 shows the damped oscillations that result when the cell concentration, φ, is reduced from 0.1 to 0.02 at $t = 0$. The value $\varphi = 0.02$ is slightly smaller than the critical cell concentration required for sustained oscillations. The evolution of the average NADH concentration shown in the top plot suggests that the cell population is becoming increasingly desynchronized. This result is consistent with experimental data [37]. The bottom plot shows the computed NADH distributions at $t = 0$, 1, 5 and 15 min. When viewed in isolation, the increasingly sharp distributions seem to indicate that the cell population is becoming synchronized. However, the sharpening actually is attributable to the NADH concentration of each cell converging to a constant value. This result shows the danger involved in interpreting snapshots of the number distribution for a transient cell population.

Figure 7 shows the onset and eventual damping of oscillations that result from a 0.1 mM pulse in the extracellular acetaldehyde/pyruvate concentration at $t = 2$ min. The initial conditions used are consistent with the perturbed model parameters and a cell concentration $\varphi = 0.02$. While they are readily computed, the distribution properties are not particularly illustrative in this case. Instead, the ensemble average concentration of each intracellular species and the extracellular acetaldehyde/pyruvate pool are shown as a function of time. The dynamic response of the average NADH concentration is very similar to that observed experimentally [31] for the same perturbation. The lack of oscillations in the extracellular acetaldehyde/pyruvate concentration is accompanied by damped oscillations in the intracellular concentrations. This result demonstrates the importance of the coupling agent on the oscillatory dynamics of the cell population.

The final test involves mixing of two populations of 500 cells which are oscillating 180 degrees out of phase. Each 500-cell ensemble has a consistent set of model parameters and initial conditions in the sense discussed above. The top plot of Figure 8 shows the evolution of the average NADH concentrations of the two cell populations prior to mixing. The average NADH concentration response of the mixed population of 1000 cells shown in the middle plot suggests that synchronization is essentially complete within 25 oscillation periods. Experimental studies [28,31] have shown that synchronization of such a mixed cell population is complete in less than ten oscillation periods. On the other hand, the simulated mixing dynamics are much faster than those obtained previously by Wolf and Heinrich with the same yeast glycolysis model but different model parameter values [17]. The faster mixing dynamics obtained here are mainly attributable to an increased value of the coupling parameter κ. The bottom plot shows computed NADH number distributions at $t = 0$, 11.25, 30 and 45 min. The initial distribution clearly shows the presence of two distinct cell subpopulations. Synchronization is reflected by the confluence of the two sub-

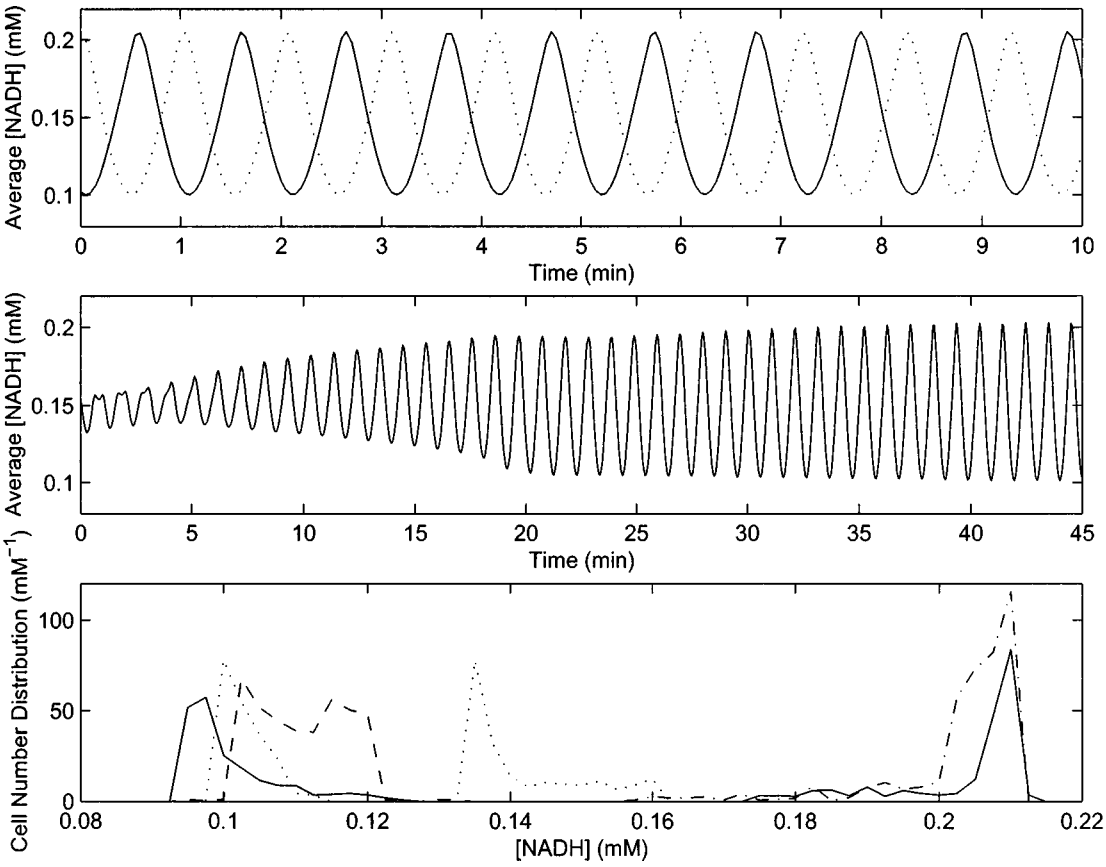

Figure 8 Cell-population synchronization following the mixing of two populations of 500 cells with random perturbations of variance 1×10^{-4} in the intracellular reaction rate constants k_1–k_6

The top plot showing the evolution of the average NADH concentrations of the two cell populations prior to mixing demonstrates that the populations are oscillating 180 degrees out of phase. The middle plot showing the evolution of the average intracellular NADH concentration of the mixed cell population consisting of 1000 cells demonstrates that synchronization is essentially complete within 25 oscillation periods. The bottom plot shows the computed NADH number distributions at 0 (——), 11.25 (· · · ·), 30 (– – – –) and 45 (–·–·) min. The discretization interval is 0.0025 mM with low and high values of 0.08 mM and 0.22 mM respectively. Synchronization of the mixed cell population is reflected by the confluence of the two subpopulations as time progresses.

populations as time progresses. The final distribution reflects a highly synchronized population in which phase variations between individual cells are very small.

SUMMARY AND FUTURE WORK

We have developed dynamic cell population models for yeast glycolysis using large ensembles of individual cell models. As compared with the more traditional PBE modelling approach, the major advantage of the cell-ensemble method is that intracellular reactions can be incorporated within a computationally tractable model. The problem of glycolytic oscillations has been used to demonstrate that the average value and the number distribution of any intracellular property captured by the individual cell model can be computed directly from the cell ensemble. We have shown that satisfactory one-dimensional NADH distributions can be obtained with 1000 individual cells. Another important conclusion is that random variations in the state and/or structure of individual cells can lead to complex population dynamics which cannot be adequately captured by small ensembles. Calculation of distribution properties involves discretization of the internal cell state under the assumption that the continuum limit represented by the PBE model can be approximated by a sufficiently large number of individual cells. A shortcoming of the proposed method is that the achievable resolution is limited by the number of cells included in the ensemble.

This paper represents our initial work on using large ensembles of individual cell models to predict cell population behaviour. Considerable research is necessary to make the cell-ensemble approach a practical tool for biochemical reactor modelling and simulation. We plan to apply the method to a rather detailed metabolic model of cell cycle related oscillations in yeast which is based on a previously published model of central carbon metabolism [4]. The construction of large cell ensembles comprised of complex individual cell models will require the development of more sophisticated computational strategies for model solution. In addition, there is need to develop more systematic methods for computing distribution properties from the cell ensemble data.

M.A.H. acknowledges the Alexander von Humboldt Foundation (Germany) for financial support. This work was completed while M.A.H. was on sabbatical leave at the Institute of Biochemical Engineering, University of Stuttgart, Stuttgart, Germany.

APPENDIX

Numerical solution of the cell ensemble model

Efficient numerical solution of the cell-ensemble model is an important issue when a large number of individual cell models is used. The model is comprised of $n = 6M+1$ coupled non-linear ODEs, where M is the number of individual cell models in the ensemble. A typical simulation involves 1000 cells ($n = 6001$), while some simulations involve as many as 5000 cells ($n = 30001$). Because we are interested in periodic solutions and the model is numerically stiff, a considerable amount of computational effort can be required to integrate the model equations over the time horizon of interest. Consequently, the dynamic simulation code should be constructed to be as efficient and robust as possible.

The simulation code was developed in FORTRAN using the variable step ODE solver DVODE [42]. Because the period of the glycolytic oscillations is approx. 1 min, a sampling time (Δt) of 0.05 min was used to achieve satisfactory signal resolution. We found that code efficiency and robustness were enhanced if the Jacobian matrix was computed analytically rather than numerically by finite difference. These calculations were straightforward given the simplicity of the model equations.

The key idea that allowed efficient solution of large cell ensembles was to approximate the full Jacobian matrix with a highly banded Jacobian matrix. The Jacobian matrix is said to be banded with lower half bandwidth m_l and upper half bandwidth m_u if the ith model equation can be written as:

$$\frac{dy_i}{dt} = f_i(y_{i-m_l}, y_{i-m_l}+1, \ldots, y_i, \ldots, y_{i+m_u}-1, y_{i+m_u}) \quad \text{(A1)}$$

where y_i is the ith dependent variable. The actual Jacobian matrix of the cell-ensemble model is not banded, owing to the presence of the acetaldehyde/pyruvate flux J_i in eqns (4) and (8) of the main paper. When these flux terms are neglected from the Jacobian calculation, the problem becomes highly banded with $m_l = m_u = 5$. We found that this simplification reduced computation time by at least an order of magnitude with no discernable effect on solution accuracy. A typical 1 h dynamic simulation with 1000 cells required less than 10 min of CPU time on a Pentium III 700 MHz processor.

Calculation of cell-distribution properties

Numerical integration of the cell-ensemble model produces a data matrix which contains the intracellular concentrations of each cell and the extracellular acetaldehyde/pyruvate concentration at each sampling point in time. This cell-ensemble data can be used to compute the average value and the number distribution of any intracellular variable. This problem was investigated previously by Shuler and Domach [14,15] in the context of computing size distributions for the binary fission organism *E. coli*. Their approach involves a number of discrete cell size classes that are chosen to provide adequate resolution of the size distribution. Each size class was populated with a number of individual cells subject to random variations in model parameters that affect the fission size. The cell-ensemble model was integrated through a number of cell cycles to yield the number of cells in each size class as a function of time. This information was used to compute steady-state and/or transient cell size distributions. However, the necessary calculations were not discussed.

Below we present a simple algorithm for computing the number distribution for any single intracellular variable such as the NADH concentration. Let $z(t)$ represent the intracellular variable for which the transient cell number distribution function $N(z,t)$ is to be computed. Consider discretization of the internal coordinate z into L intervals of width $\Delta z_l = z_l - z_{l-1}$ where $z_0 = z_{min}$ and $z_L = z_{max}$. By definition of the distribution function:

$$\int_0^\infty N(z,t)\,dz \cong \sum_{l=1}^{L} N_l(t)\Delta z_l = 1 \quad \text{(A2)}$$

where $N_l(t)$ represents the average value of $N(z,t)$ over the interval Δz_l.

Denote $\tilde{z}_m(t_k)$ as the value of the intracellular variable z produced by the mth cell at the discrete time t_k. For an ensemble consisting of M individual cells, the mean value of the intracellular variable z at time t_k is:

$$\tilde{z}(t_k) = \frac{1}{M}\sum_{m=1}^{M} \tilde{z}_m(t_k) \quad \text{(A3)}$$

An approximate distribution function is computed by partitioning the cell ensemble into the discrete intervals as follows:

$$\tilde{n}_l(t_k) = \sum_{m=1}^{M} \{S[\tilde{z}_m(t_k) - z_{l-1}] - S[\tilde{z}_m(t_k) - z_l]\}, \quad l \in [1,L] \quad \text{(A4)}$$

where $\tilde{n}_l(t_k)$ represents the number of cells with intracellular state z in the range $[z_{l-1}, z_l]$ and the unit step function is defined as:

$$S(x) = \left\{ \begin{array}{l} 0 \text{ if } x < 0 \\ 1 \text{ if } x \geqslant 0 \end{array} \right\} \quad \text{(A5)}$$

The discretized approximate number distribution function is calculated as:

$$\tilde{N}_l(t_k) = \frac{\tilde{n}_l(t_k)}{M\Delta z_l}, \quad l \in [1,L] \quad \text{(A6)}$$

If the discretization interval is sufficiently small, then a smooth continuous number distribution $\tilde{N}(z,t_k)$ can be computed from the discrete distribution values $\tilde{N}_l(t_k)$ by polynomial interpolation [16]. All the distribution calculations were performed using MATLAB.

Resolution is determined primarily by the number of cells, M, in the ensemble. As M is increased, the number of intervals, L, also can be increased such that each interval is populated with a sufficient number of cells to produce a smooth distribution function $\tilde{N}(z,t_k)$. If L is chosen too small relative to M, resolution is unnecessarily lost. On the other hand, the distribution function will be noticeably non-smooth if L is chosen too large relative to M. Unfortunately, systematic guidelines for selecting the two parameters are difficult to develop. In the present paper, dynamic simulation studies have been used to select these parameters to yield acceptable results.

REFERENCES

1 Srienc, F. (1999) Cytometric data as the basis for rigorous models of cell population dynamics. J. Biotechnol. **71**, 233–238
2 Schilling, C. H., Edwards, J. S., Letscher, D. L. and Palsson, B. O. (2001) Combining pathway analysis with flux balance analysis for the comprehensive study of metabolic systems. Biotech. Bioeng., **71**, 286–306
3 Hynne, F., Dano, S. and Sorensen, P. G. (2001) Full-scale model of glycolysis in *Saccharomyces cerevisiae*. Biophys. Chem. **94**, 121–163
4 Rizzi, M., Baltes, M., Theobald, U. and Reuss, M. (1997) *In vivo* analysis of metabolic dynamics in *Saccharomyces cerevisiae*. II. Mathematical model. Biotech. Bioeng. **55**, 592–608
5 Eakman, J. M., Fredrickson, A. G. and Tsuchiya, H. H. (1966) Statistics and dynamics of microbial cell populations. Chem. Eng. Prog. Symp. Ser. **62**, 37–49

6 Fredrickson, A. G., Ramkrishna, D. and Tsuchiya, H. M. (1967) Statistics and dynamics of procaryotic cell populations. Math. Biosci. **1**, 327–374
7 Hjortsø, M. A. and Nielsen, J. (1995) Population balance models of autonomous microbial oscillations. J. Biotechnol. **42**, 255–269
8 Mantzaris, N. V., Liou, J.-J., Daoutidis, P. and Srienc, F. (1999) Numerical solution of a mass structured cell population balance model in an environment of changing substrate concentration. J. Biotechnol. **71**, 157–174
9 Ramkrishna, D. (2000) Population Balances: Theory and Applications to Particulate Processes in Engineering, Academic Press, New York
10 Nishimura, Y. and Bailey, J. E. (1981) Bacterial population dynamics in batch and continuous-flow microbial reactors. AIChE J. **27**, 73–81
11 Nielsen, J. and Villadsen, J. (1992) Modelling of microbial kinetics. Chem. Eng. Sci. **47**, 4225–4270
12 Ataai, M. M. and Shuler, M. L. (1985) Simulation of CFSTR through development of a mathematical model for anaerobic growth of *Escherichia coli* cell population. Biotech. Bioeng. **27**, 1051–1055
13 Kim, B. G. and Shuler, M. L. (1990) A structured, segregated model for genetically modified *Escherichia coli* cells and its used for prediction of plasmid stability. Biotech. Bioeng. **36**, 581–592
14 Schuler, M. L. and Domach, M. M. (1983) Mathematical models of the growth of individual cells. In Foundations of Biochemical Engineering (Blanch, H. W., Papoutsakis, E. T. and Stephanopolous, G., eds.), pp. 93–133, American Chemical Society, Washington, D.C.
15 Domach, M. M. and Shuler, M. L. (1984) A finite representation model for an asynchronous culture of *E. coli*. Biotech. Bioeng., **26**, 877–884
16 Villadsen, J. and Michelsen, M. L. (1978) Solution of Differential Equation Models by Polynomial Approximation, Prentice-Hall, Englewood Cliffs, NJ
17 Wolf, J. and Heinrich, R. (2000) Effect of cellular interaction on glycolytic oscillations in yeast, A theoretical investigation. Biochem. J. **345**, 321–334
18 Kreuzberg, K. and Martin, W. (1984) Oscillatory starch degradation and fermentation in the green alga *Chlamydomonas reinhardii*. Biochim. Biophys. Acta. **799**, 291–297
19 Tornheim, K. (1988) Fructose 2,6-bisphosphate and glycolytic oscillations in skeletal muscle extracts. J. Biol. Chem. **263**, 2619–2624
20 Chance, B., Williamson, J. R., Jamieson, D. and Schoener, B. (1965) Properties and kinetics of reduced pyridine nucleotide fluorescence of the isolated and *in vivo* rat heart. Biochem. Z. **341**, 357–377
21 Ibsen, K. H. and Schiller, K. W. (1967) Oscillations of nucleotides and glycolytic intermediates in aerobic suspensions of Ehrlich ascites tumor cells. Biochim. Biophys. Acta **799**, 291–297
22 Rapp, P. E. (1987) Why are so many biological systems periodic? Prog. Neurobiol. **29**, 261–273
23 Das, J. and Busse, H.-G. (1991) Analysis of the dynamics of relaxation type oscillation in glycolysis of yeast extracts. Biophys. J. **60**, 363–379
24 Betz, A. and Chance, B. (1965) Phase relationship of glycolytic intermediates in yeast cells with oscillatory metabolic control. Arch. Biochem. Biophys. **109**, 585–594
25 Das, J. and Busse, H.-G. (1985) Long term oscillations in glycolysis. J. Biochem. (Tokyo) **97**, 719–727
26 Ghosh, A. and Chance, B. (1964) Oscillations for glycolytic intermediates in yeast cells. Biochem. Biophys. Res. Commun. **16**, 174–181
27 Teusink, B., Bakker, B. M. and Westerhoff, H. V. (1996) Control of frequency and amplitudes is shared by all enzymes in three models for yeast glycolytic oscillations. Biochim. Biophys. Acta **1275**, 204–212
28 Ghosh, A. K., Chance, B. and Pye, E. K. (1971) Metabolic coupling and synchronization of NADH oscillations in yeast cell populations. Arch. Biochem. Biophys. **145**, 319–331
29 Richard, P., Diderich, J. A., Bakker, B. M., Teusink, B., van Dam, K. and Westerhoff, H. V. (1994) Yeast cells with a specific cellular make-up and an environment that removes acetaldehyde are prone to sustained glycolytic oscillations. FEBS Lett. **341**, 223–226
30 Richard, P., Teusink, B., Westerhoff, H. V. and van Dam, K. (1993) Around the growth phase transition *S. cerevisiae*'s make-up favors sustained oscillations of intracellular metabolites. FEBS Lett. **318**, 80–82
31 Richard, P., Bakker, B. M., Teusink, B., van Dam, K. and Westerhoff, H. V. (1996) Acetaldehyde mediates the synchronization of sustained glycolytic oscillations in populations of yeast cells. Eur. J. Biochem. **235**, 238–241
32 Goldbeter, A. and Lefever, R. (1972) Dissipative structures for an allosteric model. Application to glycolytic oscillations. Biophys. J. **12**, 1302–1315
33 Selkov, E. E. (1975) Stabilization of energy charge, generation of oscillation and multiple steady states in energy metabolism as a result of purely stoichiometric regulation. Eur. J. Biochem. **59**, 151–157
34 Bier, M., Bakker, B. M. and Westerhoff, H. V. (2000) How yeast cells synchronize their glycolytic oscillations. A perturbation analytic treatment. Biophys. J. **78**, 1087–1093
35 Wolf, J. and Heinrich, R. (1997) Dynamics of two-component biochemical systems in interacting cells, Synchronization and desynchronization of oscillations and multiple steady states. Biosystems **43**, 1–24
36 Wolf, J., Passarge, J., Somsen, O. J. G., Snoep, J. L., Heinrich, R. and Westerhoff, H. V. (2000) Transduction of intracellular and intercellular dynamics in yeast glycolytic oscillations. Biophys. J. **78**, 1145–1153
37 Aon, M. A., Cortassa, S., Westerhoff, H. V. and van Dam, K. (1992) Synchrony and mutual stimulation of yeast cells during fast glycolytic oscillations. J. Gen. Microbiol. **138**, 2219–2227
38 Mantzaris, N. V., Daoutidis, P. and Srienc, F. (2001) Numerical solution of multivariable cell population balance models. I, Finite difference methods. Comp. Chem. Eng. **25**, 1411–1440
39 Mantzaris, N. V., Daoutidis, P. and Srienc, F. (2001) Numerical solution of multivariable cell population balance models. III, Finite element methods. Comp. Chem. Eng. **25**, 1463–1481
40 Zhu, G.-Y., Zamamiri, A. M., Henson, M. A. and Hjortsø, M. A. (2000) Model predictive control of continuous yeast bioreactors using cell population models. Chem. Eng. Sci. **55**, 6155–6167
41 Hatzis, C., Srienc, F. and Fredrickson, A. G. (1995) Multistaged corpuscular models of microbial growth: Monte Carlo simulations. Biosystems **36**, 19–35
42 Brown, P. N., Byrne, G. D. and Hindmarsh, A. C. (1989) VODE, a variable coefficient ODE solver. SIAM J. Sci. Stat. Comput. **10**, 1038–1051

Received 3 July 2002/14 August 2002; accepted 2 September 2002
Published as BJ Immediate Publication 2 September 2002, DOI 10.1042/BJ20021051